

Micron-scale deformation: a coupled in-situ study of strain bursts and acoustic emission

Ádám István Hegyi,^{1,*} Péter Dusán Ispánovity,¹ Michal Knappek,² Dániel Tüzes,¹ Krisztián Máthis,² František Chmelík,² Zoltán Dankházi,¹ Gábor Varga,¹ and István Groma¹

¹*Department of Materials Physics, Eötvös University,*

Pázmány Péter sétány 1/a, H-1117 Budapest, Hungary

²*Charles University in Prague, Faculty of Mathematics and Physics*

Department of Physics of Materials, Ke Karlovu 5 121 16 Prague 2

(Dated: April 8, 2016)

Plastic deformation of micron-scale crystalline materials differ considerably from bulk ones, because it is characterized by random strain bursts. To obtain a detailed picture about this stochastic phenomenon, micron sized pillars have been fabricated and compressed in the chamber of a SEM. An improved FIB fabrication method is proposed to get non-tapered micro-pillars with a maximum control over their shape. The in-situ compression device developed allows high accuracy sample positioning and force/displacement measurements with high data sampling rate. The collective avalanche-like motion of dislocations appears as stress drops on the stress-strain curve. To confirm that these stress drops are directly related to dislocation activity, and not to some other effect, an acoustic emission transducer has been mounted under the sample to record emitted acoustic activity during strain-controlled compression tests of Al-5% Mg micro-pillars. The correlation between the stress drops and the acoustic emission signals indicates that indeed dislocation avalanches are responsible for the stochastic character of the deformation process.

PACS numbers: 64.70.Pf, 61.20.Lc, 81.05.Kf, 61.72.Bb

I. INTRODUCTION

During the past decades miniaturizing mechanical and electronic devices inspired research on determining the mechanical properties of micron sized specimens¹⁻⁵. The vast majority of micro-electromechanical sensors contain micrometer size pieces, for instance, accelerometer measures the buckling of a micro-cantilever or chemical and biological sensors use cantilever transducers as a platform^{6,7}. In order to be able to design devices that are even smaller, the detailed physical properties of the deformation processes should be studied.

The plastic deformation of crystalline materials is usually caused by the motion of the dislocations. In macroscopic samples, due to the large number of dislocations, the stress-strain response

of the material is smooth allowing to predict the properties of the material with a high accuracy. In contrast, at the micrometer scale the inhomogeneity of the dislocation microstructure is in the order of the sample size resulting non-deterministic response due to the stochastic motion of dislocations^{8–12}. So, in order to design new microscopic devices the mechanical properties of materials have to be described by a statistical approach at this scale.

The first evidence of intermittent crystal plasticity was obtained on ice single crystals by detecting strong acoustic emission signals during creep deformation^{13,14}. A decade ago by compressing pure single crystalline Ni micro-pillars Dimiduk et. al. found that instabilities in the form of strain jumps dominate micrometer scale crystal plasticity^{15–17} raising the questions (i) what is the limit between microscopic and macroscopic deformation, and (ii) how one can define material strength parameters, like flow stress, for micron-scale objects^{18–20}.

Due to its statistical nature to determine the properties of micro-deformation a vast amount of micrometer size samples are needed. One of the easiest and most frequently applied method to fabricate them is focused ion beam (FIB) milling²¹, with the main advantage that one can meanwhile visually check the process of ion milling. To shorten the fabrication time of the micro-pillars several different growing (FIB-less) methods were developed^{22,23}. These, however, do not allow to produce pillars from any type of material, and to have control over the initial dislocation content in the sample. Moreover, for pillars produced by growing the connecting force between the substrate and the micro-pillar itself can be rather weak.²⁴

To fabricate micro-pillars by FIB milling two approaches are commonly applied: “lathe” and “top-down” millings²⁵. Lathe-milling uses ion beam (almost) perpendicular to the axis of the micro-pillar’, and the pillar is rotated around to get the cylindrical shape. Usually this procedure is used on the side of a thin layer of a crystal material. In the top-down technique the pillar axis is parallel to the ion beam, the ions etch the surface of the sample prepared. In this case, however, the height of the micro-pillar and its tapering are poorly controlled. The new method outlined below combines the advantages of both fabrication techniques. With this procedure a non-tapered micro-pillar can be obtained anywhere on the surface of a bulk material, and much less preparation time is required²⁶. Moreover, by this technique it is possible to investigate in-used parts in a quasi non-destructive way.

In the studies presented our main goal was to get an insight into the fundamentals of plastic deformation at the micrometer scale. The new fast micro-pillar fabrication procedure developed gives us the chance to perform a statistical analysis of the deformation processes. This is essential because during an individual compression experiment the stress varies intermittently (see below),

meaning that the dislocation system gives stochastic response to the acting force^{11,14,16,27,28}. As a result of this defining material parameters from a unique measurement is impossible. So, hardness, or strain hardening can only be calculated from a statistical analysis^{20,28}.

The compression tests were performed on Al-5% Mg alloy micro-pillars fabricated onto the surface of the bulk material. An important feature of this alloy is that it shows the Portevin-Le Chatelier (PLC) effect^{29–32}. So, even for bulk samples, intermittent stress-strain response is observed which is related to the pile-up and break out of the dislocations from the solute atom atmosphere acting as junctions for mobile dislocations^{31,32}. This mechanism also generates strong acoustic signals with energies slightly higher than those caused by dislocation avalanches. Since the stress drops caused by PLC and dislocation avalanches are clearly distinguishable, the tests on this material allowed us to determine the sensitivity of our acoustic emission detector setup.

II. SAMPLE PREPARATION

Prior to fabrication the size of the micro-pillar has to be decided. Since in this study we are interested in the collective dislocation phenomena, we have to have enough dislocations in the system initially. On the same time the sample size should not be too large to hinder the stress drops. Normally in fcc metals like Al the dislocation density varies between $10^{11} - 10^{14} \text{ m}^{-2}$, therefore, the average spacing between dislocations is about $3 - 0.1 \mu \text{ m}$. Since the dislocations tend to form a cell like structure with a characteristic size of about 10 times the dislocation spacing, the pillar size is selected to be in the order of the cell size.

In-situ micro-pillar deformation tests demand very careful and precise sample preparation. To get the required surface properties, orientation, and initial dislocation density the following steps were performed: after a short etching the Al-5% Mg sample was electropolished in perchloric electrolyte *D2* solution with 60 mA/mm^2 current density. The lattice orientation was measured using electron back-scattered diffraction (EBSD). The sample was cut by electric discharge machining (EDM) to have a surface orientation $\langle 1, 2, 3 \rangle$. After this, another electropolishing step was made, then the sample was heat treated for 72 hours at 200°C . After the heat treatment, the surface was electropolished again with 30 mA/mm^2 and the orientation was checked again by EBSD. The sample was pre-deformed parallel to the $\langle 1, 2, 3 \rangle$ axis to 20 MPa. The initial dislocation density was measured by TEM and X-ray line profile analysis, and was found to be $2 \times 10^{13} \text{ m}^{-2}$. Taking this value into account, a pillar geometry with rectangular cross section of $4 \times 4 \mu \text{m}^2$ was selected with a height of $12 \mu \text{m}$ corresponding to a aspect ratio about 3:1:1 commonly applied in earlier

studies.

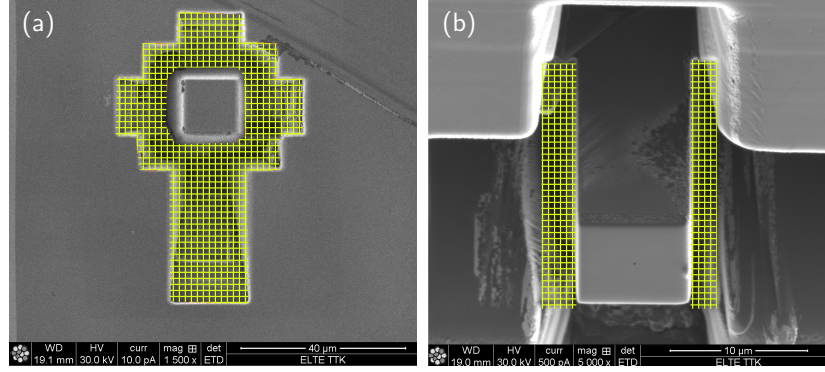


FIG. 1: a) The initial FIB milling step marked by the grid to fabricate the “raw” pillar and the hole around it, that is necessary to carry out the compression test. At this milling step 30 nA ion current is applied. b) The second finalizing milling step with 45° ion direction angle (see Fig. 2, too). The area removed by this step is marked by the grid. The ion current is 5 nA. Both pictures are taken from the ion direction.

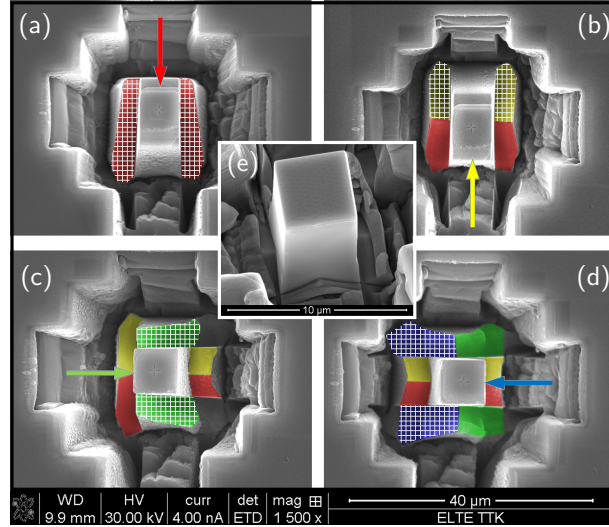


FIG. 2: The details of the second finalizing step of the micro-pillar fabrication procedure with an ion current of 5 nA. a) After the first step seen in Fig. 1 the sample is tilted by 45° resulting a tilted ion beam direction. After this, two rectangular FIB patterns (marked by the red grid) are used to get the surface marked by red. b) As a next step the sample is rotated by 180°, and two rectangular FIB patterns are used again to get the surface marked by yellow. With a rotation by 90°, and repeating the two previous steps the surfaces marked by green c) and blue d) are obtained. With these a square shaped pillar is achieved. In order to get a pillar with smooth surface and practically no tapering the process is repeated with ion currents 1 nA, and 100 pA too. The final pillar obtained is seen in the inset e).

After the above mentioned sample preparation processes a “surrounding hole” was milled by 30 nA ion current around the pillar. The FIB milling pattern used is marked by the grid in Fig. 1/a. The sample was oriented so that the normal vector of the surface was parallel to the ion beam direction. Then a thin Pt layer was deposited onto the top surface of the micro-pillar. The cap helps the ion beam to fabricate smooth side surface of the pillar and due to its amorphous structure it is very hard which can help to eliminate effects related to the missalignment of the compressing tip (see below). To do the next step the stage is tilted by 7° . Due to the 52° ion-electron beam angle this result in a 45° ion beam direction compared to the surface normal. To avoid flaws originating from the non-repeatability of the microscope stage during positioning a $2\text{ }\mu\text{m}$ size cross was drawn to the geometric center of the top surface of the micro-pillar. After this the milling steps explained in the caption of Fig. 2 were performed. In order to further decrease tapering³³, a final “polishing like” step is performed with 30 pA ion beam over-tilted by 1° compared to the pillar axis.

Apart from the first step explained above the fabrication works with high surface angle. This increases the effectiveness of the milling by a factor of 2.5-3 compared to the perpendicular beam setup commonly used³⁴. The 45° milling direction applied in the second phase lets us to fabricate micro-pillars anywhere on the flat sample surface.

It has to be mentioned, that the Ga ion beam forms an irradiated skin on the micro-pillar. The slightly tilted final “polishing” step with the reduced 10 pA ion current and the lowered acceleration voltage (to 20 kV or 10 kV) decreases the thickness of this layer leading to a negligible effect at pillar size used³⁵.

To sum up the most important advantages of the milling procedure proposed are: (i) pillars can be fabricated at any position on the surface, (ii) the preparation is touchless, so, the damage or the deformation of the pillar can be avoided during the whole production process, and (iii) effects related to tapering and Ga implantation can be neglected.

III. IN-SITU DEVICE

An in-situ micro-mechanical test requires the testing device to be placed inside the chamber of the microscope. We have developed such a compression device for a FEI Quanta 3D scanning electron microscope. The sketch of the device is shown in Fig. 3.

Two linear ultrasonic motors are used for the X and Y positioning of the sample. The AE transducer is mounted on the top of the two stages. In Z direction two stages are used. One is a linear step-motor stage used for the “raw” motion of the compressing tip to get it close to the

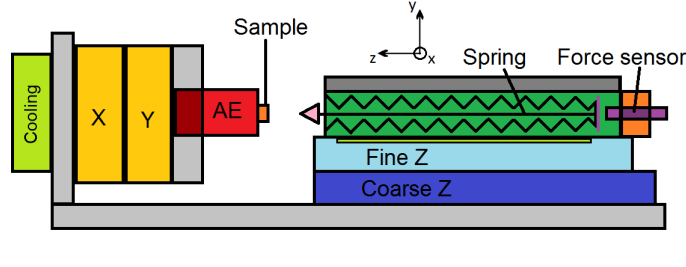


FIG. 3: Sketch of the in-situ device NANOTEST.

sample. The other one mounted on the linear step-motor stage is a piezoelectric positioning (PEP) stage with about 0.1 nm resolution. During the actual compression test only this stage is moved. To measure the external force a standard spring mounted on the PEP stage is used with strong transverse but very weak longitudinal stiffness. The elongation E of the spring is measured by a capacitive sensor with 0.1 nm resolution. If the PEP stage is moved by the distance P , and the capacitive sensor measures E elongation than the sample deformation is $D = P - E$, and the acting force is $F = SE$, where S is the stiffness of the spring. The pillar compression is performed using a flat punch diamond tip. It should be mentioned that to avoid the charging of the compressing head in the SEM a tip doped by boron has to be used.

For being able to measure instabilities related to PLC effect and dislocation avalanches it is crucial to have a fast enough feedback controlling system and minimum of $1kHz$ data collection rate. These are achieved by an analogous PID type feedback electronics and a fast 16bit AD converter.

The range and the resolution parameters of the device are summarized in Table 1.

TABLE I: Parameters of the nanodeformation device

| Part name | Total range | Resolution | Accuracy |
|--------------|------------------|---------------------|---------------------|
| X and Y | ± 8 mm | $0.5 \mu\text{m}$ | $0.01 \mu\text{m}$ |
| Z coarse | 9 mm | $2 \mu\text{m}$ | $0.5 \mu\text{m}$ |
| Z fine | $35 \mu\text{m}$ | 1 nm | 0.1 nm |
| Force sensor | 20/50 mN | $1/2.5 \mu\text{N}$ | $1/2.5 \mu\text{N}$ |

To achieve these resolutions the thermal and elastic elongation of the different parts have to be negligible during the typically few minutes of the measuring time. For this reason, several different additional parts are added to the compression device. One main problem is to reduce the heat produced by the motors of the stages. The Quanta 3D has an environmental stage with a Peltier

sample holder to set the sample temperature. The cold point of this Peltier stage is mounted to the bottom of the device. By this, the temperature is stabilized at 15 °C. Another important issue that needs to be eliminated is the vibration of the spring of the force sensor arising due to the lack of air, that is, damping. To avoid this rather disturbing effect strong permanent magnets are placed close to the lamellae of the force measuring spring providing the necessary damping due to the eddy currents.

IV. ACOUSTIC EMISSION MEASUREMENT

An Acoustic Emission (AE) measuring system was also employed to study the dynamic processes occurring during the plastic deformation of micropillars. Acoustic emissions are transient elastic waves generated by the rapid release of energy from localized sources within the material. Thus, AE signals are generated where sudden localized structural changes take place, like dislocation motion or twinning. So, it provides information about the dynamic phenomena involved in plastic deformation³⁶.

In bulk materials, a direct correlation of AE parameters with the stress-strain curves can reveal the activation of different deformation mechanisms^{37–40}. It is important to note that the collective motion of at least several tens of dislocations is necessary in order to obtain a detectable AE signal⁴¹. So, in terms of AE, a motion of a single dislocation is typically “silent” and, in turn, a detectable AE signal (if caused by dislocation activity) reflects the cooperative character of dislocation motion.

Crackling or avalanche-like type of plasticity is not only characteristic for micron-scale objects, but also for bulk samples³⁹. In this case the AE technique exhibits a great potential to provide information on these dynamic processes invisible on the deformation curves. To the knowledge of the authors, the study presented in the paper is the first attempt to record AE signals during the micro-pillar compression.

The AE signal measurement was performed by a Physical Acoustics PCI-2 acquisition board based on a continuous storage of AE signals with 2 MHz sampling rate. The full scale of the A/D converter was ± 10 V. The AE was amplified by 60 dB in the frequency range of 100 – 1200 kHz. The background noise during the tests did not exceed 24 dB. Due to this small noise level the detecting threshold level was set to 26 dB. The AE was recorded simultaneously during uni-axial compression of the micro-pillar.

A rectangular piece of material (with pillar samples fabricated onto its surface) was attached directly to the AE transducer using a metallic spring. In addition, the acoustic contact was

improved by means of a vacuum grease.

The load as a function of the time together with the acoustic emission signal obtained on a Al-5% Mg micro-pillar at a constant compressive strain rate is plotted in Fig. 4. As it is expected the sample shows the well known PLC effect. The stress drops at the very beginning of the deformation and just before plastic yielding (enlarged in inset a)) can be attributed to the breakout of dislocations from the surrounding solute atoms. As it is seen in inset a) just at the onset of the stress drop a large acoustic emission signal is detected.

At the micro-pillar size ($4 \times 4 \times 12 \mu m^3$) used in the test the PLC effect competes with the intermittent dislocation motion (dislocation avalanches). This dual effect destroys the well-known periodic stress drop structure of the deformation curve, and randomly distributed avalanches can be found. In inset b) the waveform of the acoustic signal can be seen. The large peaks on the acoustic emission signal are generated by collective motion of many dislocations.

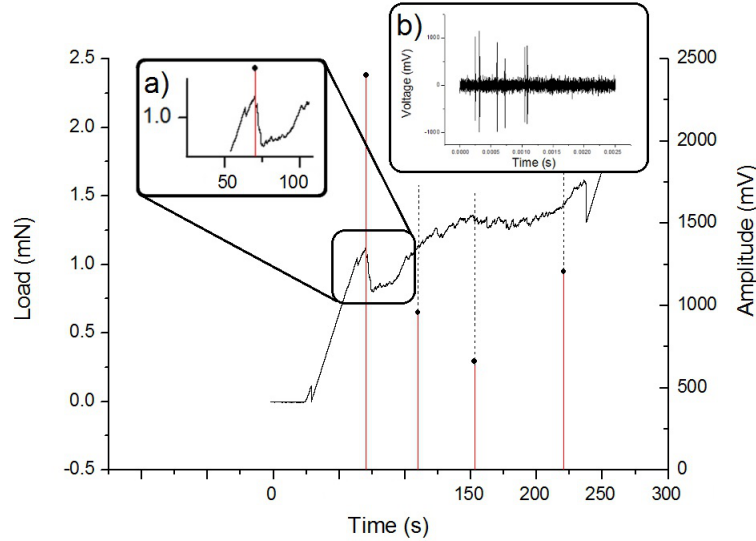


FIG. 4: Load versus time curve obtained by a micro-pillar compression with constant strain rate. In inset a) a stress drop is enlarged. Inset b) shows the waveform of an acoustic signal.

V. SUMMARY

In order to understand in detail the deformation properties of micron sized objects experiments carried out on a large ensemble of specimens are needed. The pillar fabrication method presented in the paper is considerably faster than those applied earlier. This opens the possibility to carry

out investigations that can reveal the statistical properties of micron scale plasticity. The results obtained indicate that detecting acoustic emission signal related to the cooperative motion of dislocations is feasible even from the small (about $100 \mu\text{m}^2$) volume of a micro-pillar.

Acknowledgments

Financial supports of the Hungarian Scientific Research Fund (OTKA) under contract numbers K-105335 and PD-105256 and of the European Commission under grant agreement No. CIG-321842 are also acknowledged. PDI is supported by the János Bolyai Scholarship of the Hungarian Academy of Sciences.

* Electronic address: hegyi@metal.elte.hu

- ¹ C. A. Volkert and E. T. Lilleodden, *Philosophical Magazine* **86**, 5567 (2006).
- ² K. Ng and A. Ngan, *Acta Materialia* **56**, 1712 (2008).
- ³ C. Zhou, I. J. Beyerlein, and R. LeSar, *Acta Materialia* **59**, 7673 (2011).
- ⁴ M. Zaiser, J. Schwerdtfeger, A. Schneider, C. Frick, B. G. Clark, P. Gruber, and E. Arzt, *Philosophical Magazine* **88**, 3861 (2008).
- ⁵ O. Kraft, P. A. Gruber, R. Mönig, and D. Weygand, *Annual review of materials research* **40**, 293 (2010).
- ⁶ N. Yazdi, F. Ayazi, and K. Najafi, *Proceedings of the IEEE* **86**, 1640 (1998).
- ⁷ N. V. Lavrik, M. J. Sepaniak, and P. G. Datskos, *Review of scientific instruments* **75**, 2229 (2004).
- ⁸ J. Weiss and D. Marsan, *Science* **299**, 89 (2003).
- ⁹ M. Zaiser, F. M. Grasset, V. Koutsos, and E. C. Aifantis, *Physical review letters* **93**, 195507 (2004).
- ¹⁰ M. Zaiser and P. Moretti, *Journal of Statistical Mechanics: Theory and Experiment* **2005**, P08004 (2005).
- ¹¹ M.-C. Miguel, A. Vespignani, M. Zaiser, and S. Zapperi, *Physical review letters* **89**, 165501 (2002).
- ¹² S. Zapperi, *The European Physical Journal B* **85**, 1 (2012).
- ¹³ J. Weiss, F. Lahaie, and J. R. Grasso, *Journal of geophysical research-solid earth* **105**, 433 (2000).
- ¹⁴ M.-C. Miguel, A. Vespignani, S. Zapperi, J. Weiss, and J.-R. Grasso, *Nature* **410**, 667 (2001).
- ¹⁵ M. D. Uchic, D. M. Dimiduk, J. N. Florando, and W. D. Nix, *Science* **305**, 986 (2004).
- ¹⁶ D. M. Dimiduk, C. Woodward, R. LeSar, and M. D. Uchic, *Science* **312**, 1188 (2006).
- ¹⁷ M. D. Uchic, P. A. Shade, and D. M. Dimiduk, *Annual Review of Materials Research* **39**, 361 (2009).
- ¹⁸ E. Arzt, *Acta materialia* **46**, 5611 (1998).
- ¹⁹ J. R. Greer and J. T. M. De Hosson, *Progress in Materials Science* **56**, 654 (2011).
- ²⁰ P. D. Ispánovity, Á. Hegyi, I. Groma, G. Györgyi, K. Ratter, and D. Weygand, *Acta Materialia* **61**, 6234 (2013).
- ²¹ S. Reyntjens and R. Puers, *Journal of Micromechanics and Microengineering* **11**, 287 (2001).

- ²² A. T. Jennings, M. J. Burek, and J. R. Greer, *Physical review letters* **104**, 135503 (2010).
- ²³ M. J. Burek and J. R. Greer, *Nano letters* **10**, 69 (2009).
- ²⁴ G. Moser, H. Felber, B. Rashkova, P. Imrich, C. Kirchlechner, W. Grosinger, C. Motz, G. Dehm, and D. Kiener, *Practical Metallography* **49**, 343 (2012).
- ²⁵ J. Hütsch and E. T. Lilleodden, *Scripta Materialia* **77**, 49 (2014).
- ²⁶ S. Wurster, R. Treml, R. Fritz, M. Kapp, E. Langs, M. Alfreider, C. Ruhs, P. Imrich, G. Felber, and D. Kiener, *Practical Metallography* **52**, 131 (2015).
- ²⁷ M. Zaiser, *Advances in physics* **55**, 185 (2006).
- ²⁸ P. D. Ispánovity, I. Groma, G. Györgyi, F. F. Csikor, and D. Weygand, *Physical review letters* **105**, 085503 (2010).
- ²⁹ T. Tabata, H. Fujita, and Y. Nakajima, *Acta Metallurgica* **28**, 795 (1980).
- ³⁰ N. Chinh, F. Csikor, Z. Kovács, and J. Lendvai, *Journal of Materials Research* **15**, 1037 (2000).
- ³¹ J. Gubicza, N. Q. Chinh, Z. Horita, and T. Langdon, *Materials Science and Engineering: A* **387**, 55 (2004).
- ³² A. Yilmaz, *Science and Technology of Advanced Materials* (2016).
- ³³ J. Li, T. Malis, and S. Dionne, *Materials characterization* **57**, 64 (2006).
- ³⁴ T. Ishitani, K. Umemura, T. Ohnishi, T. Yaguchi, and T. Kamino, *Journal of electron microscopy* **53**, 443 (2004).
- ³⁵ J. R. Greer, H. Espinosa, K. Ramesh, and E. Nadgorny, *Applied Physics Letters* **92**, Art (2008).
- ³⁶ C. Heiple and S. Carpenter, *Journal of Nuclear Materials* **149**, 168 (1987).
- ³⁷ J. Bohlen, F. Chmelík, P. Dobroň, D. Letzig, P. Lukáč, and K. Kainer, *Journal of alloys and compounds* **378**, 214 (2004).
- ³⁸ P. Dobroň, F. Chmelík, J. Bohlen, K. Hantzsche, D. Letzig, and K. Ulrich Kainer, *International Journal of Materials Research* **100**, 888 (2009).
- ³⁹ J. Weiss, T. Richeton, F. Louchet, F. Chmelik, P. Dobron, D. Entemeyer, M. Lebyodkin, T. Lebedkina, C. Fressengeas, and R. J. McDonald, *Physical Review B* **76**, 224110 (2007).
- ⁴⁰ Z. Kovács, M. Ezzeldien, K. Máthis, P. Ispánovity, F. Chmelík, and J. Lendvai, *Acta Materialia* **70**, 113 (2014).
- ⁴¹ C. Scruby, H. Wadley, K. Rusbridge, and D. Stockham-Jones, *Metal Science* **15**, 599 (1981).